

# Diagnosis of Multiple Open-circuit and Short-circuit Faults in Three-phase Multicellular Inverter Based on Sliding Mode Observer

Fatma Khater<sup>1</sup>, Abderrezak Aibeche<sup>1</sup>, Sid Ali Fellag<sup>1</sup>, Mohamed Zinelabidine Doghmane<sup>2</sup> and Hamza Akroum<sup>1</sup>

<sup>1</sup>Laboratoire d'Automatique Appliquée (LAA). Département d'automatisation et électrification des procédés, Faculté des hydrocarbures et de la chimie (FHC), Université M'hamed Bougara - Boumerdès, Boumerdes 35000 Algérie.

<sup>2</sup>Département Evaluation des Réservoirs, Direction des Opérations D'Exploration, Division Exploration, Sonatrach, Hassi Messaoud 30500, Ouergla, Algérie.

## Abstract

The reliability and security of multicellular converters have become crucial tools for safeguarding electrical power conversion and ensuring the continuity of electrical drives. This concern has always been paramount in numerous industrial applications. Ensuring the reliability, continuity, and robustness of the three-phase multicellular inverter critically depends on accurately diagnosing faults in insulated gate bipolar transistor (IGBT) switches; these failures carry both technical and economic consequences for electrical system conversion. Therefore, detecting and diagnosing faults is crucial to preserving converters against these potential issues. This study aims to investigate the operational behavior of the three-phase multicellular inverter under normal and faulty conditions, more precisely focusing on open-circuit and short-circuit faults in converter switches. To achieve this objective, the paper introduces a fault diagnosis technique based on a sliding mode observer for power switches in the three-phase multicellular inverter. The research is divided into two main sections. The initial segment concentrates on the aspects of sliding mode control, aiming to attain regulated output voltages, output currents, and floating capacitor voltage. This control strategy is essential for maintaining a stable and consistent operation of the inverter. The second segment focuses on fault diagnosis, analyzing the impact of a defective three-phase multicellular inverter on the overall functionality of the electrical system. The performance of the proposed algorithm is assessed and validated through simulations in the MATLAB/Simulink environment.

**Keywords:** *Three-phases multicellular inverter, faults diagnosis, open-circuit fault, short-circuit fault, sliding mode observer.*

## 1. Introduction

Power electronics have evolved in the last few decades due to the development of semiconductor power components used in high-speed switching converter structures and the appearance of new converter structures. Few structures can handle high switching frequencies, while others are designed to transfer high power levels

(i.e., multi-level, multi-cell, and multi-cell stepped structures) [1].

Among these systems, multicellular converters, first developed in the 1990s by *H. Foch* and *T. Meynard*, are based on the series association of elementary commutation cells [2]. This topology ensures that voltage constraints are distributed across the different low semiconductor components connected in series.

Corresponding author: Fatma KHATER ([f.khater@univ-boumerdes.dz](mailto:f.khater@univ-boumerdes.dz))

Received: 29 October 2024; Revised: 19 February 2025; Accepted: 4 March 2025; Published: 17 March 2025

© 2025 The Author(s). This work is licensed under a Creative Commons Attribution 4.0 International License

The multicellular structure necessitates using floating capacitors, whose terminal voltages must be controlled and maintained at well-defined levels to maintain these advantages. The serial multicellular converter's structure is adaptable to all configurations, including mounting as a chopper or an inverter. These converters are an attractive solution for high-power applications in many industrial applications of power systems supply [3]. These converters are widely used in industry and research. This use has led to the development of specific control laws to ensure correct operation. In the literature, several approaches have been considered to develop methods of controlling and observing unknown variables of multicellular converters.

The modeling approach constitutes a crucial step in synthesizing control laws and observers [4]; modeling accuracy relies on the specific objectives that need to be achieved. For this reason, we can find different models for the same process, and the choice between them will depend on its use and control objective. The modeling of the multicellular converter is generally complex; indeed, the latter contains continuous variables (currents and voltage) and discrete variables (switches). The literature has three models: the average, harmonic, and the instantaneous models [1], [5]. The control of static converters hybridizes automatic control and power electronics, striving to enhance converter performance by adapting control to its structure, ultimately improving energy transmission to the load. The characteristics of a series multicellular inverter allow for ensuring the balance and evolution of the voltage across the capacitors by acting directly on the inverter control signal. Multicellular inverters have been successfully controlled in an open loop structure using the PWM (Pulse Width Modulation) control technique [4].

Nevertheless, there are instances where PWM control fails to regulate capacitor voltages at specific operating points, risking damage to the converter. Therefore, designing closed-loop control strategies to guarantee the inverter's proper operation becomes crucial. Various techniques have been suggested to address this issue, including linear and non-linear control methods [6], [7]. In [8], *Emelyanov* proposed and developed the first works on sliding mode variable structure control systems in the early 1950s. However, only in the 1980s did sliding mode control (SMC) of variable structure systems become interesting and attractive.

The multicellular converters are highly sensitive to power semiconductor failure, which can be classified as open-circuit (OC) and short-circuit (SC) faults [9], [10]. It would reduce the system's performance and force it to disconnect from the network. On one hand, SCF is deemed the most severe type of fault, capable of causing substantial damage and prompting an immediate system shutdown. On the other hand, OCF usually results in partial or complete loss of operation in one of the IGBTs within the static converter, leading to performance degradation [11], [12]. The SC-type fault of a switch appears when one of the two switches remains continuously in the ON state. The SCF occurs when the second switch is, in turn, controlled to close. This fault occurs due to a failure in the control of the transistors (driver failure, control card failure, connection problem between the control card and the driver) or due to physical failure of the piece of silicon caused by exceeding the temperature. Power switch SCF faults are challenging to handle due to subjecting the damaged component to high current, high voltage, and excessive local temperatures. Without a protection mode, this fault can spread and damage the other switch on the same phase in a matter of microseconds. An OC-type fault typically results in the total or partial failure of one of the IGBTs constituting the static converter. It is imperative to detect and compensate switch failures regardless of their nature to prevent the degradation of system performance and to avoid the propagation of failures and the generation of additional issues within the energy conversion chain. Failure to detect and subsequently compensate for the fault could destroy the inverter.

A fault diagnosis method is crucial to mitigate these risks and enable the multicellular inverter to continue operating under nominal conditions until future maintenance can be conducted. Fault diagnosis plays a critical role in enhancing reliability, ensuring service continuity, and reducing maintenance costs of power electronics. It has been a significant focus of research in recent years. [13] introduces a fault diagnosis method for OCF in inverters, using a voltage-extended state observer designed for the dynamic mixed logic model. Open circuit faults are detected based on the residual phase voltage between the observed and actual voltage. In [14], a technique for diagnosing SCF and OCF faults of the three-phase inverter is presented; this technique aims to identify and locate faults in the IGBT of the three-phase inverter,

which is based on the maximum single voltage of the inverter output and compared to its reference. In [15], a sliding mode observer-based fault detection method is developed for a multi-cell converter of four quadrants. [16] discusses a sliding mode observer-based approach for open-circuit fault detection of switch faults in a multilevel converter. A fault diagnosis of OCF and SCF faults in a multi-cell converter based on a sliding mode observer is proposed in [17]; this diagnostic approach is based on a first-order sliding mode switched observer. Authors in [18] introduced a fault diagnosis method for multilevel-multicell converters based on a sliding mode controller and an adaptive threshold; this fault detection method is based on monitoring the output voltage and current. Authors in [19] presented fault diagnosis methods for short circuits and open circuits; they proposed a classification and diagnosis approach based on applying a gate signal to each switch; this method uses only current magnitude data while applying a voltage vector to detect faulty switches.

In this paper, we present a fault diagnosis method based on sliding mode observer for detecting, identifying, and isolating OCF and SCF faults in the three-phase multicellular inverter. This manuscript is organized as follows. After introducing the subject, section 2 presents the three-phase multicellular inverter model. In section 3, the sliding mode controller is presented and tested. The fault diagnosis method proposed has been demonstrated in section 4, and finally, in section 5, concluding remarks are presented with recommendations for future research.

## 2. Three-Phases Multicellular Inverter Model

The modeling approach is very important for synthesizing control laws and observers. A three-phase multicellular inverter consists of three single-phase multicellular inverters grouped in parallel and controlled so that the output three voltages are shifted by 120 degrees.

Figure 1 shows a representative diagram of a floating capacitor three-phase multicellular inverter. It supplies a three-phase load with resistance  $R$ , and inductance  $L$ .  $E$  represents the DC input voltage. It is a hybrid system in which continuous (voltages and currents) and discrete (binary switches) variables evolve.

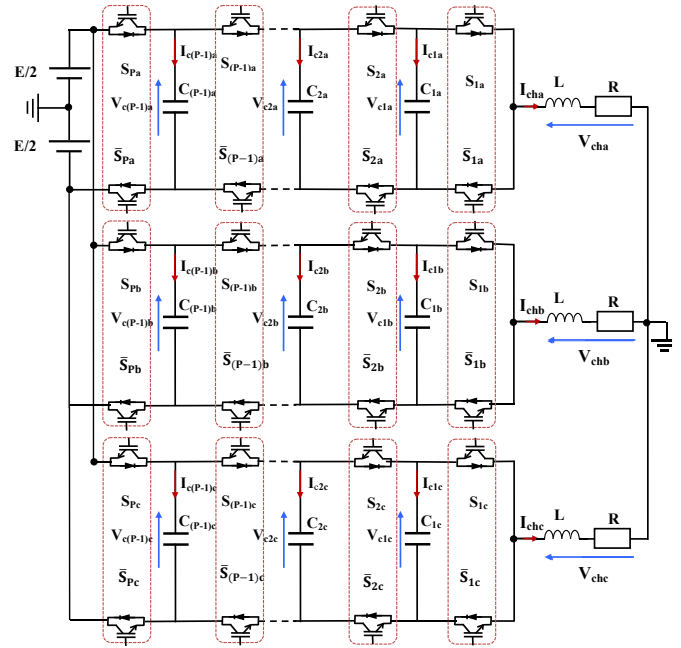


Figure 1. Representative diagram of a three-phase multicellular inverter.

The following definitions are offered with reference to phase (a), but are valid for all phases. Each phase of the inverter is composed of  $p$  elementary switching cells connected in series, with each cell consisting of two complementary switches. It is controlled by a binary signal  $u_k$ ; when the cell's upper switch is conducting, this signal equals 1, and 0 when the cell's lower complementary switch is conducting. These cells are connected to the R-L load in series and separated by floating capacitors.

There are  $p-1$  floating voltage sources [7], [20]. There are  $n_{\text{cells}} + 1$  voltage levels available at the output of each phase. A representative schematic of a single phase of a three-phases multicellular inverter is shown in Figure 2.

Each cell is surrounded by two voltage sources  $V_{Ck}$  and  $V_{Ck-1}$ ; for:  $k=1 \dots n-1$ . With  $V_{C0}=0$ ,  $V_{Cp}=E$ ; so:

$$V_{\text{Cell}_k} = V_{Ck} - V_{Ck-1} \quad (1)$$

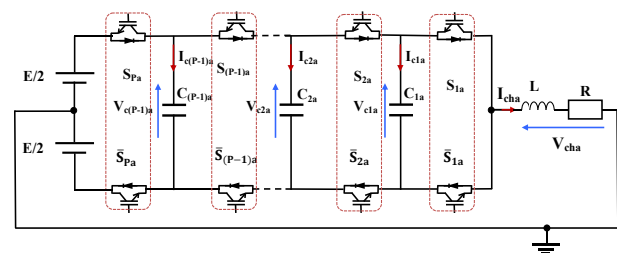


Figure 2. Structure of a single phase of a three-phases multicellular inverter.

An equal distribution of voltage constraints on each cell must be imposed to assure normal functioning i.e.

$$V_{C_k} = k \cdot \frac{E}{P} \quad (2)$$

In addition, the applied voltage to the load is given by:

$$V_{ch}(t) = \sum_{k=1}^P S_k \cdot V_{cell_k} \quad (3)$$

The voltage on the capacitor  $C_k$  is related to the current  $I_{ck}$  by:

$$i_{C_k}(t) = (S_{cell_{k+1}} - S_{cell_k}) \cdot i_{ch}(t) \quad (4)$$

$$\frac{dV_{C_k}}{dt} = \frac{(S_{cell_{k+1}} - S_{cell_k})}{C_k} \cdot i_{ch}(t) \quad (5)$$

The given expression describes the behavior of all states of the converter. To deduce the output voltage, Kirchhoff's law is applied. Therefore, the load voltage is given by:

$$V_{ch}(t) = \sum_{k=1}^P (V_{C_k}(t) - V_{C_{k-1}}(t)) \cdot S_{cell_k} \quad (6)$$

By grouping these expressions in the form of equations of states, we obtain:

$$\begin{aligned} \frac{dV_{C_1}}{dt} &= \frac{1}{C_1} (S_2 - S_1) \cdot i_{ch} \\ \frac{dV_{C_2}}{dt} &= \frac{1}{C_2} (S_3 - S_2) \cdot i_{ch} \\ &\vdots \\ \frac{dV_{C_{P-1}}}{dt} &= \frac{1}{C_{P-1}} (S_P - S_{P-1}) \cdot i_{ch} \\ \frac{di_{ch}}{dt} &= \frac{1}{L} (S_1 - S_2)V_{C_1} + \frac{1}{L} (S_2 - S_3)V_{C_2} + \dots \\ &\quad + \frac{1}{L} (S_{P-1} - S_P)V_{C_{P-1}} + \frac{S_P}{L} E \\ &\quad - \frac{R}{L} i_{ch} \end{aligned} \quad (7)$$

From the given differential equations, we establish a state representation with the state variables being the floating voltages  $V_{ck}$  and the load current  $i_{ch}$ , which takes the following form:

$$\dot{X} = AX + BU \quad (8)$$

With:  $X = [V_{C_1}, V_{C_2} \dots, V_{C_{P-1}}, i_{ch}]^T$ ;  $U$ : the control vector.

### 3. Control of Three-Phases Multicellular Inverter

A three-phase multicellular inverter's control system must guarantee the regulation of output currents and voltages in each phase while ensuring an even distribution of stresses on each switch. Several control approaches have been developed and documented in the literature for these inverters. PWM control is an open loop control called natural control that guarantees the correct operation of the inverter studied and the balancing of the voltages at the terminals of the capacitors. However, it is necessary to develop closed-loop control strategies to ensure the stability, robustness, and continued correct operation of this inverter, such as the application of the sliding mode control technique, which takes into account the evolution of output voltages and currents as well as the capacitor voltages. Applying these control techniques to our three-phase multicell series inverter piques our interest in this section.

#### 3.1. Open loop control

Pulse Width Modulation (PWM) is a simple and efficient control method that operates in an open loop, ensuring the proper functioning of the inverter and maintaining the voltages across the terminals of floating capacitors. The principle of this strategy is the comparison of a modulating signal and a triangular carrier; the intersection of these two signals generates the control signal for each cell; these command orders must be out of phase by an angle of  $\delta = 2\pi/p$ . Each carrier has a value between 0 and 1, and the function that allows these carriers to be generated is given by equation 9 [15], [21].

$$\begin{aligned} t_{r1} &= \frac{2}{\pi} \arcsin[\cos(2\pi f_{dec}t)] \\ t_{r1} &= \frac{2}{\pi} \arcsin[\cos(2\pi f_{dec}t - \delta)] \\ &\vdots \\ t_{rp} &= \frac{2}{\pi} \arcsin[\cos(2\pi f_{dec}t - (p-1)\delta)] \end{aligned} \quad (9)$$

The principle of PWM control for a multicell phase of a three-phase inverter is depicted in Figure 3. In this technique, control commands for each cell are derived from the intersection of a triangular carrier and a sinusoidal modulation signal. Due to the need to control the various cells that make up the multicellular phase, a significant amount of carrier is required. The regular

phase shift of the triangular carriers allows, on the one hand, the multilevel output voltage to reach its intermediate levels; on the other hand, this regular phase shift makes it possible to multiply the apparent frequency of the output voltage.

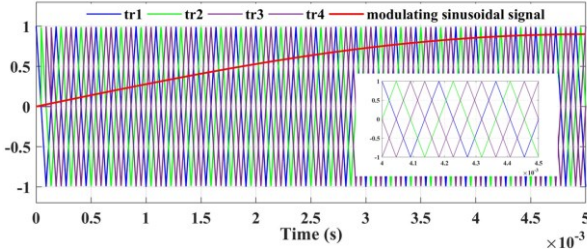


**Figure 3.** Principle of the PWM control for a single phase of the three-phases multicellular inverter.

In Figure 4, the evolution of the output voltage and current of the three-phase multicell inverter is represented. The three phases exhibit a 120-degree phase shift, with each phase having five voltage levels.

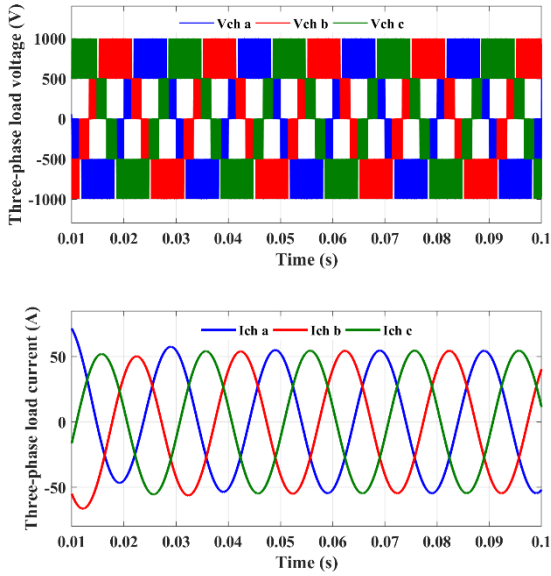


**Figure 4.** Load voltages and currents of the three-phase multicellular inverter.

### 3.2. Sliding mode controller

Sliding Mode Control (SMC) is a type of nonlinear controller that utilizes Lyapunov's method and is known for its robust performance in the face of model uncertainties and external disturbances [22]. The primary objectives of control using sliding modes can be summarized in two key points: first, to create a surface  $S$  such that all system trajectories follow the desired behavior for tracking, regulation, and stability; second, to

establish a control law  $U$  that attracts and maintains all state trajectories on this sliding surface [23], [24]. The multicellular inverter is a nonlinear system with a variable structure and multiple inputs; implementing sliding mode control involves defining a sliding surface for each switching cell. Additionally, it is essential to associate these surfaces with an appropriate control law that ensures the stability and continuous operation of the converter.

We consider the system defined by equation (8); the dimension of the surface vector  $S$  aligns with that of the control vector  $U$ .

To ensure the convergence of a state variable  $x$  towards its reference values  $x_{ref}$ , various forms of sliding surfaces have been introduced. Typically, the selection of a surface is based on the error in the controlled variable denoted as  $e(x)$ , where  $e(x) = x_{ref} - x$ . Thus, we define  $p$  sliding surfaces as follows:

$$\begin{aligned} S_1 &= V_{C_{ref1}} - V_{C_1} \\ S_2 &= V_{C_{ref2}} - V_{C_2} \\ &\vdots \\ S_p &= i_{ch_{ref}} - i_{ch} \end{aligned} \quad (10)$$

In order to verify the convergence condition, we use the Lyapunov approach. The Lyapunov's function is chosen as follows:

$$V(X) = \frac{1}{2} S^2(X) \quad (11)$$

To ensure the decrease of the Lyapunov function, it is sufficient to guarantee that its derivative is negative.

$$V(X) = \dot{S}(X) \cdot S(X) < 0 \quad (12)$$

The structure of the sliding mode controller consists of two components  $U = U_{eq} + U_n$ .

$U_{eq}$  ensures that the controlled variable is maintained on the sliding surface defined by  $S = 0$ . This command is derived from the observation that the surface's derivative is zero. The value of  $U_n$  is determined to satisfy the convergence condition. During the sliding surface phase and steady state, the surface remains at zero, allowing us to derive the expression for the equivalent control.

$$U_{eq} = - \left[ \frac{\delta S}{\delta X} \cdot B(X) \right]^{-1} \cdot \left[ \frac{\delta S}{\delta X} \cdot A(X) \right] \quad (13)$$

During the convergence mode, and by replacing the equivalent command with its expression, the attractiveness condition becomes:



$$S(X) \cdot \frac{\partial S}{\partial X} B(X) \cdot U_n < 0 \quad (14)$$

To fulfill the attractiveness condition, the sign of  $U_n$  must be opposite that of  $S(X) \cdot \frac{\partial S}{\partial X} B(X)$ . The proposed form of the discrete command  $U_n$  is:

$$U_n = K_i \text{sign}(S(X)) \quad (15)$$

$K$  is a constant, and the selection of this constant  $K$  is highly impactful.

Subsequent Figure 5 and Figure 6 depict the load voltage, load current, and floating capacitor voltage of a single phase of the three-phase multicell inverter controlled by SMC, respectively.

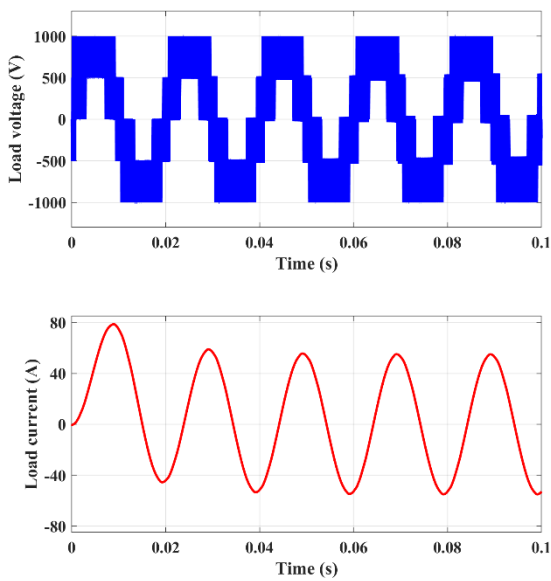


**Figure 5.** Load voltage and load current of a single phase of the three-phase multicell inverter controlled by SMC.

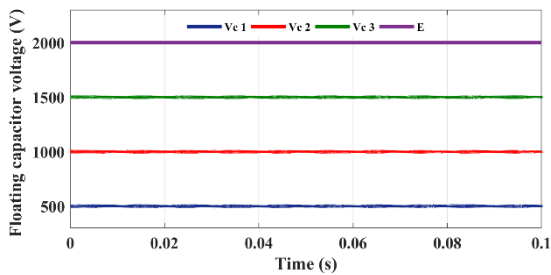


**Figure 6.** Floating capacitor voltage of a single phase of the three-phase multicell inverter controlled by SMC.

The simulation results of this control strategy applied to the studied converter, shown in Figures 5 and 6, show that the output voltages and currents reach their desired reference values, as well as an equitable distribution of the voltages at the terminals of the floating capacitors.

#### 4. Fault Diagnosis Based on Sliding Mode Observer

With many sensitive components, the risk of failure in a multicell-multilevel converter is much higher. In the presence of a failure of a semiconductor device, a multilevel converter will operate with distorted output voltages and currents. Multilevel inverter fault diagnosis has emerged as an intriguing topic in the field of inverter fault diagnosis. This work focuses on the faults that occur in the power switches of a multicell inverter, which can be categorized into two types: short circuit (SC) faults and open circuit (OC) faults.

The fundamental concept behind using an observer for fault detection is to estimate the system's outputs based on measurements and subsequently construct the residual by appropriately weighing the error between the output estimate and the actual output. The residual is then scrutinized for the possibility of faults by employing an adaptive threshold. Specific decision rules can then be applied to determine whether a fault has occurred [25], [26].

A diagnostic technique based on a sliding mode observer is proposed for detecting and identifying IGBT faults in a three-phase multicellular inverter. This observer generates parameter estimates that serve as diagnostic signals, using a developed mathematical model's input and output signals. These estimated signals are compared with their regular counterparts to identify their differences. The detected differences act as signatures for fault diagnosis. The proposed sliding mode observer can be described as follows:

$$\begin{aligned} \dot{\hat{V}}_{C_1} &= \frac{[S_2 - S_1]}{C} \cdot \hat{i}_{ch} \\ \dot{\hat{V}}_{C_2} &= \frac{[S_3 - S_2]}{C} \cdot \hat{i}_{ch} \\ &\vdots \\ \dot{\hat{V}}_{C_{p-1}} &= \frac{[S_p - S_{p-1}]}{C} \cdot \hat{i}_{ch} \\ \hat{i}_{ch} &= \frac{[S_1 - S_2]}{L} \cdot \hat{V}_{C_1} + \frac{[S_2 - S_3]}{L} \cdot \hat{V}_{C_2} + \dots \\ &\quad + \frac{[S_{p-1} - S_p]}{L} \cdot \hat{V}_{C_{p-1}} + \frac{1}{L} S_p \\ &\quad \cdot E - \frac{R}{L} \cdot \hat{i}_{ch} - \frac{1}{2L} \cdot E \end{aligned} \quad (16)$$

$$\begin{aligned}
\begin{bmatrix} \hat{V}_{C_1} \\ \hat{i}_{ch} \end{bmatrix} &= \begin{pmatrix} 0 & \frac{[S_2 - S_1]}{C} \\ \frac{[S_1 - S_2]}{L} & \frac{R}{L} \end{pmatrix} \cdot \begin{bmatrix} \hat{V}_{C_1} \\ \hat{i}_{ch} \end{bmatrix} + \hat{\Gamma}_1 \\
&\quad + \begin{bmatrix} \theta_1 \text{sign}(\tilde{V}_{C_1}) \\ \theta_2 \text{sign}(\tilde{i}_{ch}) \end{bmatrix} \\
\begin{bmatrix} \hat{V}_{C_2} \\ \hat{i}_{ch} \end{bmatrix} &= \begin{pmatrix} 0 & \frac{[S_3 - S_2]}{C} \\ \frac{[S_2 - S_3]}{L} & \frac{R}{L} \end{pmatrix} \cdot \begin{bmatrix} \hat{V}_{C_2} \\ \hat{i}_{ch} \end{bmatrix} + \hat{\Gamma}_2 \\
&\quad + \begin{bmatrix} \theta_1 \text{sign}(\tilde{V}_{C_1}) \\ \theta_2 \text{sign}(\tilde{i}_{ch}) \end{bmatrix} \\
&\vdots \\
\begin{bmatrix} \hat{V}_{C_p} \\ \hat{i}_{ch} \end{bmatrix} &= \begin{pmatrix} 0 & \frac{[S_p - S_{p-1}]}{C} \\ \frac{[S_{p-1} - S_p]}{L} & \frac{R}{L} \end{pmatrix} \cdot \begin{bmatrix} \hat{V}_{C_{p-1}} \\ \hat{i}_{ch} \end{bmatrix} \\
&\quad + \hat{\Gamma}_k + \begin{bmatrix} \theta_1 \text{sign}(\tilde{V}_{C_{p-1}}) \\ \theta_2 \text{sign}(\tilde{i}_{ch}) \end{bmatrix}
\end{aligned} \tag{17}$$

Where:

$$\begin{aligned}
\hat{\Gamma}_1 &= \frac{1}{L} (S_2 - S_3) \cdot \hat{V}_{C_2} + \dots + \frac{1}{L} (S_{p-1} - S_p) \\
&\quad \cdot \hat{V}_{C_{p-1}} + \frac{1}{L} \left( S_p - \frac{1}{2} \right) \cdot E \\
\hat{\Gamma}_2 &= \frac{1}{L} (S_1 - S_2) \cdot \hat{V}_{C_1} + \dots + \frac{1}{L} (S_{p-1} - S_p) \\
&\quad \cdot \hat{V}_{C_{p-1}} + \frac{1}{L} \left( S_p - \frac{1}{2} \right) \cdot E \\
&\vdots \\
\hat{\Gamma}_k &= \frac{1}{L} (S_1 - S_2) \cdot \hat{V}_{C_1} + \dots + \frac{1}{L} (S_{p-2} - S_{p-1}) \\
&\quad \cdot \hat{V}_{C_{p-2}} + \frac{1}{L} \left( S_p - \frac{1}{2} \right) \cdot E
\end{aligned} \tag{18}$$

With:  $\theta_1$  and  $\theta_2$  are the observer gains (large constant), and the residual  $\tilde{V}_{Ci}$

$$\tilde{V}_{Ci} = V_{Ci} - \hat{V}_{Ci} \tag{19}$$

Sign (x) is the sign function, that is defined as:

$$\text{sign}(x) = \begin{cases} 1 & x > 0 \\ 0 & x = 0 \\ -1 & x < 0 \end{cases} \tag{20}$$

The basic concept behind the fault diagnosis method based on sliding mode observer is to compare the observed states with simulated states of a three-phase multicellular inverter. If there is a discrepancy between these states for a certain period, it indicates that a fault has occurred. This occurrence triggers a procedure that

involves assumptions, modifications, and evaluations to identify the fault, as shown in Figure 7.

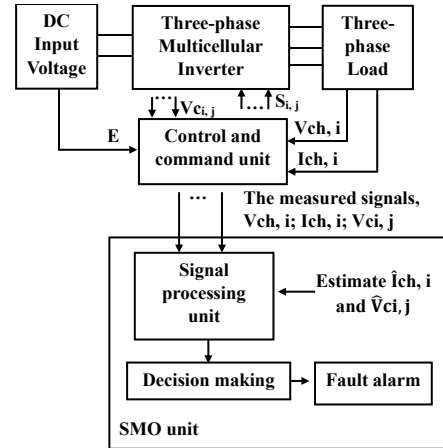


**Figure 7.** Diagram of the fault diagnosis method based on sliding mode observer.

The introduced sliding mode observer demonstrates excellent state estimation performance; the estimated currents ideally attend to the measured currents and the voltages at the terminals of the floating capacitors, as illustrated in Figure 8.

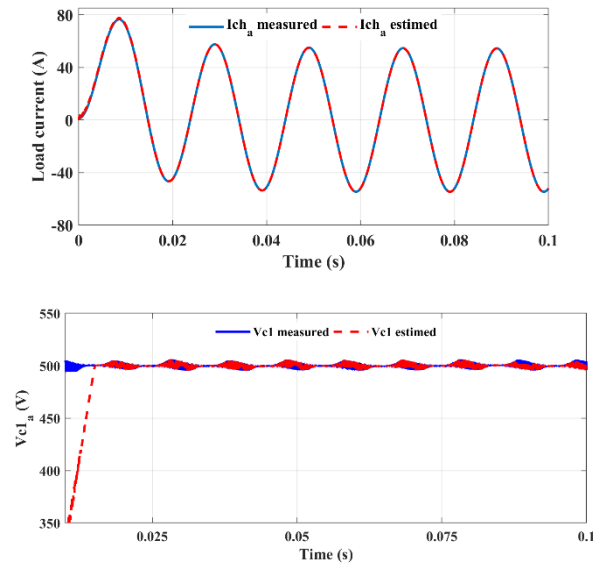


**Figure 8.** The load current and voltage of the 1st floating capacitor measured and estimated for a single phase of the three-phase four-cell inverter.

In normal operating mode (without faults), the output currents and voltages achieve their reference values. However, when a fault occurs in the IGBTs of the multicellular inverter's arm, the system degrades, distorting the output voltages and currents in the affected phase of the three-phase multicellular inverter.

#### 4.1. The diagnosis strategy of the OCF and SCF in the three-phase multicellular inverter

The proposed fault diagnosis technique consists of two steps: the first involves detecting the faulty phase, and the second focuses on detecting and localizing the faulty IGBT.

##### 4.1.1. Detection of the faulty phase

In a healthy operating condition (without faults), a three-phase inverter's three phases should ideally be out of phase by an angle of 120 degrees. Under these circumstances, the waveforms of the voltages and currents are identical, indicating no issues affecting their output. However, if one of the three-phase voltage or current signals shows distortion compared to the others, it suggests a fault affecting the IGBTs in the corresponding phase of the inverter.

##### 4.1.2. Identification of the faulty cells

In the event of a fault affecting an IGBT in one phase of the inverter, the first step is identifying the faulty phase. Once the faulty phase is determined, the next stage is to locate the specific faulty cell within that phase. This can be done by monitoring the voltage of the floating capacitor associated with the affected cell. The voltage of the capacitor linked to the faulty cell is expected to show noticeable distortion compared to the voltages of the other capacitors in the system. When an OCF occurs at the upper IGBT switch (USF) (e.g., the first phase), the current cannot flow through the IGBT S1, which means that the positive current of phase A must be zero, the negative current can flow through the IGBT S2. The current value will be non-positive when the OCF occurs at the upper stage. Similarly, if an OCF occurs at the lower IGBT switch (LSF), the current value will be non-negative after the fault is triggered. These clues are used to detect and localize faulty IGBT.

##### 4.1.3. Isolation of the faulty cells

After identifying the faulty component, the fault isolation process focuses on separating it from the rest of the circuitry to prevent any potential damage to the system. This damage may involve deactivating or

bypassing the defective component while ensuring the remainder of the system functions properly.

#### 4.2. Simulations and discussion results

In this section, a three-phase multicellular inverter circuit is simulated under the MATLAB/SIMULINK 2018a environment using the parameters' values summarized in Table 1.

**Table 1.** Operating parameters of the three-phases multicellular inverter.

Parameter	Description	Values
$V_{in}$ [V]	Input DC voltage	2000
$C_{i,j}$ [F]	Capacitor	$3e^{-4}$
$R_j$ [ $\Omega$ ]	Load resistance	5
$L_j$ [H]	Load inductance	$5e^{-2}$
$f_{PWM}$ [kHz]	The switching frequency	5.5
$T_e$ [s]	The switching period	$1e^{-6}$

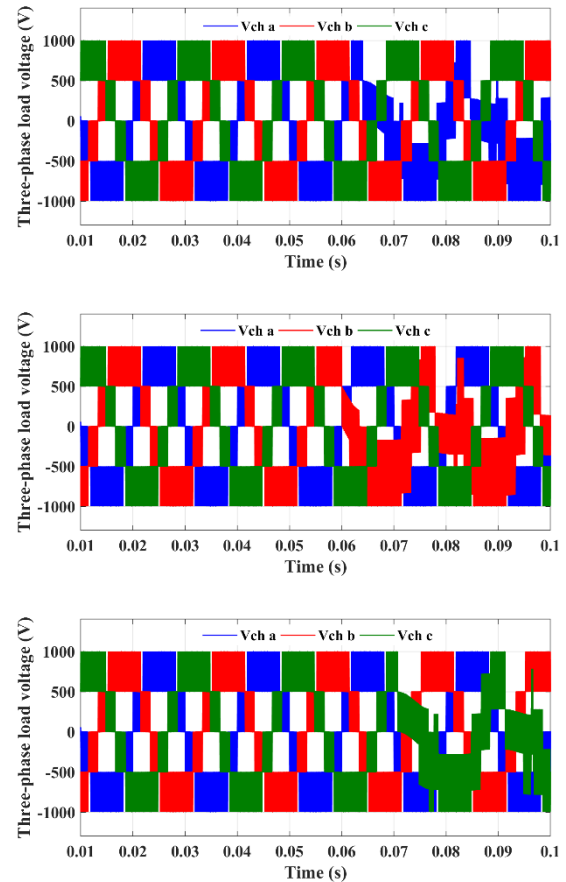


**Figure 9.** The variations of Three-phase voltages during the appearance of an OCF on the inverter phases.



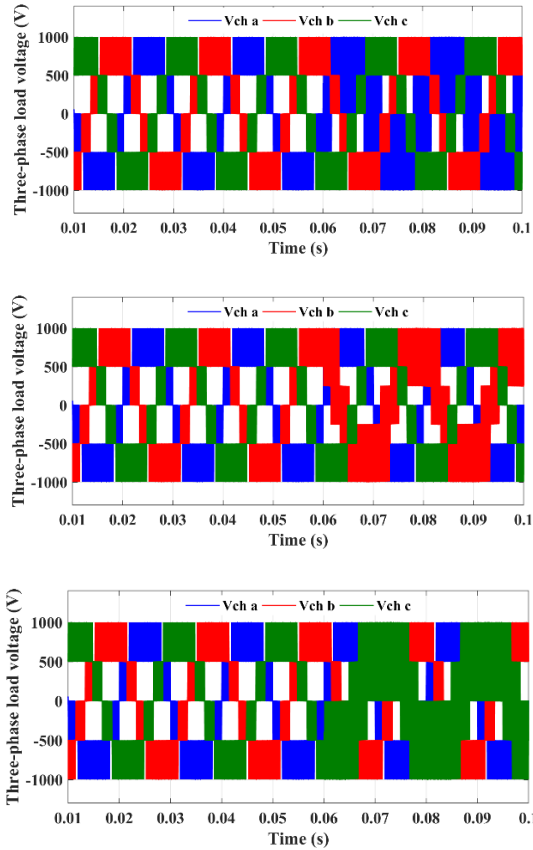


**Figure 10.** The variations of Three-phase voltages during the appearance of an SCF on the inverter phases.

The main objective of fault diagnosis is to promptly detect and identify different types of failures at their early stages. Building on the previous analysis, we will focus on the faults affecting our inverter. We initiate by identifying the faulty phase. The subsequent Figures illustrate the dynamics of the output voltage of the three-phase multicellular inverter under fault conditions, specifically an OCF fault and SCF fault occurring on the IGBTs of the inverter. Subsequently, we will present the dynamics of the output currents of the three-phase multicellular inverter in the presence of these faults.

Before defects occur, the three-phase voltage waveforms appear identical and exhibit a phase shift of 120 degrees without distortion. At time  $t=0.06$  (s), a fault is detected in one phase of the three-phase multicellular inverter. This fault detection results in distortion of the output voltage in the faulty phase, in contrast to the voltage signals from the other phases. From this observation, we can identify the defective phase in the inverter, as shown in Figure 9 and Figure 10.

After identifying the faulty phase, the next step is to locate the defective cell within that phase.

#### 4.2.1. Case 1: Open-Circuit faults

In Figure 11, we plotted the output voltages and currents during an open-circuit (OCF) fault on the IGBT of the first phase of the inverter at time  $t = 0.05$  (s). The figures illustrate the faulty phase by showing noticeable deformations in the output voltage and current waveforms. Additionally, we observe that the voltage of the floating capacitor corresponding to the defective cell is distorted when the fault occurs.

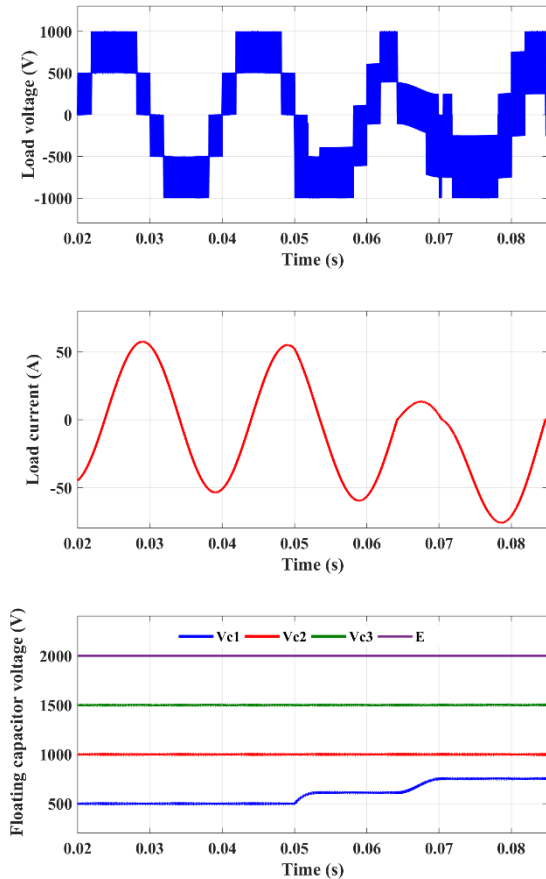


**Figure 11.** Evolution of the load voltage; load current; floating capacitor voltage; of the 1st phase of the inverter during the appearance of OCF fault in the US.

The defective cell can be identified by observing the voltage degradation across the floating capacitors. This degradation is evident when the positive alternation of the current in the first phase is canceled, indicating that the fault originates in the upper stage. Conversely, a fault occurs in the IGBT of the lower stage. In that case, the measured current will be canceled during the negative alternation, leading to load voltage distortions, as illustrated in Figure 12.

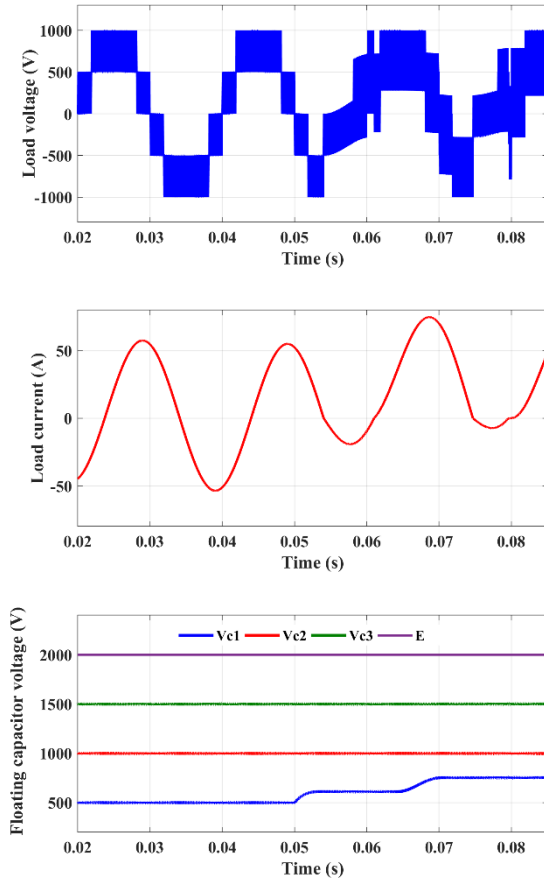


**Figure 12.** Evolution of the load voltage; load current; floating capacitor voltage; of the 1st phase of the inverter during the appearance of OCF fault in the lower LS.

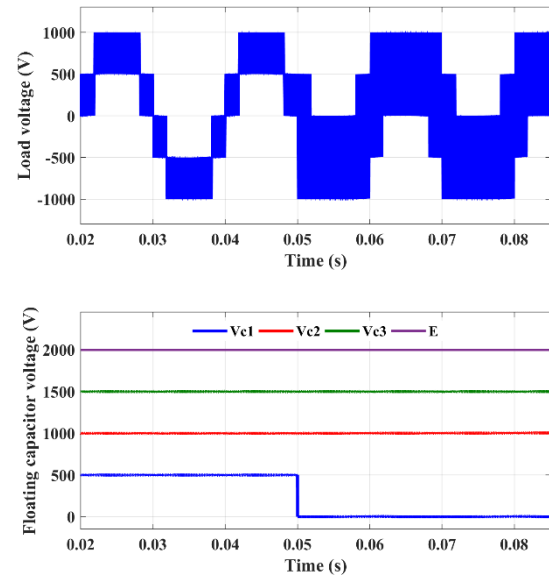
To analyze the impact of an OCF on a three-phase multicellular inverter, we applied open-circuit faults to various IGBT transistors within the inverter. The results were consistent with previous observations. When an OCF occurs in an IGBT of one phase, the degraded operation is evident in the distorted load voltages of the affected phase. The measured load currents are nullified during the positive half-period if the fault is at the upper stage (US) and during the negative half-period if the fault is at the lower stage (LS). Additionally, the voltage across the floating capacitors connected to the faulty cell experiences significant fluctuations upon the occurrence of the fault, as shown in Table A1.

Table A1 illustrates the voltage fluctuations across the floating capacitors corresponding to different positions of OCF fault. To precisely identify the defective cell, observing the apparent deterioration of voltages across the floating capacitors is possible. Upon an OCF fault in the  $k$ th cell, notable variations are observed in the voltages of

the two adjacent floating capacitors. The capacitor  $C_k$  acquires a voltage, while the adjacent capacitor  $C_{k-1}$  experiences a proportional voltage reduction corresponding to the acquired energy.

#### 4.2.2. Case 2: Short -Circuit faults

In Figure 13, we present the output voltages during a short-circuit (SCF) fault occurring on the IGBT of the first phase of the three-phase inverter at time  $t = 0.05$  (s). These Figures clearly illustrate the faulty phase by showing deformations in the output voltage waveform. Additionally, it is noted that the voltage of the floating capacitor associated with the defective cell becomes distorted when the fault occurs.



**Figure 13.** Evolution of the load voltage and the floating capacitor voltage; of the 1st phase of the three-phase four-cells inverter during the appearance of SCF fault.

SCF faults were introduced to various IGBT transistors constituting the inverter to evaluate the impact of SCF on the three-phase multicellular inverter. The results obtained are consistent with those reported previously. The defective cell can be identified by observing the voltage degradation across the floating capacitors. When an SCF fault occurs in the IGBT of one phase of the three-phase inverter, the degraded state is indicated by deformations in the load voltages of the faulty phase. The voltage across the floating capacitors associated with the defective cell undergoes substantial fluctuations upon the occurrence of the fault, as illustrated in Table A2.

Table A2 depicts the voltage fluctuations across the floating capacitors corresponding to different SCF fault positions. We can observe the significant voltage deterioration across the floating capacitors to identify the defective cell. When a SCF fault occurs in the  $k^{\text{th}}$  cell, substantial variations are evident in the voltages of the two adjacent floating capacitors. The voltage of capacitor  $C_k$  experiences a sudden decrease, while the adjacent capacitor  $C_{k-1}$  receives a proportional voltage corresponding to the energy lost from capacitor  $C_k$ .

#### 4.2.3. OC and SC faults detection and identification

Detecting OCF and SCF faults in a three-phase multicellular inverter is crucial for maintaining the safe and reliable operation of power electronic systems. Typically, this procedure involves observing and analyzing different electrical parameters. In this section of the study, the method employed for detecting and identifying defects is the sliding mode observer described previously. The proposed observer generates parameter estimation signals; the distinction between these and measured signals is employed as a distinctive marker for detecting faults. By observing the signals of the output's voltages and current as well as the floating capacitors voltages of the three-phase multicellular inverter, a significant understanding of the inverter's functioning can be obtained. Sudden fluctuations in these signals can act as indicators of faults. The  $\hat{V}_{Ci}$  and  $\hat{i}_{Ch}$  are the observed signals of  $V_{Ci}$  and  $i_{Ch}$ .

Once a fault occurs, the measured and estimated load current and floating capacitor voltages are observed. The fault will probably degrade the load voltage and current, as well as the floating capacitor voltage associated with the faulty cell, beyond the normal operating range. Monitoring The measured and estimated signals. If there is a significant difference between these values, this indicates a fault. The residuals, the estimation errors, are then analyzed to detect and isolate the faults. Thresholds are designed and applied to the residuals formed for fault diagnosis. In this step, we construct the residual, i.e., the differences between the measurement of the system output and its estimated values. The residual  $r_i$  can be expressed as follows:

$r_i = y_i - \hat{y}_i$ , where  $y_i$  is the measured value and  $\hat{y}_i$  is the estimated value.

At time  $t = 0.05$  (s), an OCF fault occurred in the IGBT associated with the first cell of phase (a). This fault resulted in a degraded operating condition characterized by significant distortions in both the load voltages and currents, as shown in Figure 11 and Figure 12. Figure 14 and Figure 16 illustrate the measured and estimated signals of the load current and the voltage across the floating capacitors of the faulty phase in the three-phase inverter.

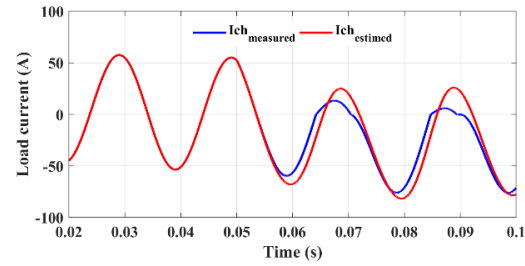


**Figure 14.** The measured and estimated load current of the faulty phase during OCF.

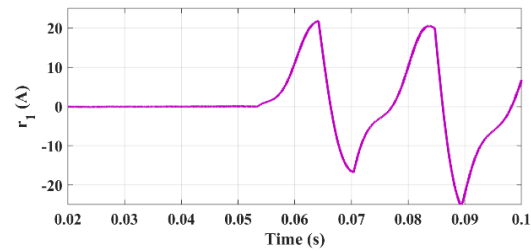


**Figure 15.** The residuals of the measured and estimated load current of the faulty phase during the OCF.

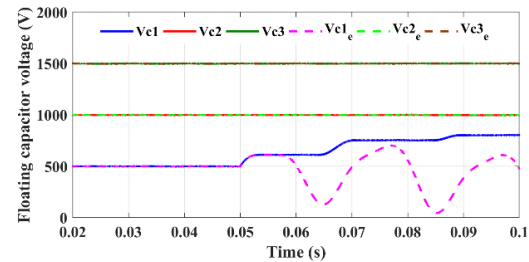


**Figure 16.** The measured and estimated voltages of the floating capacitors of the faulty phase during OCF.

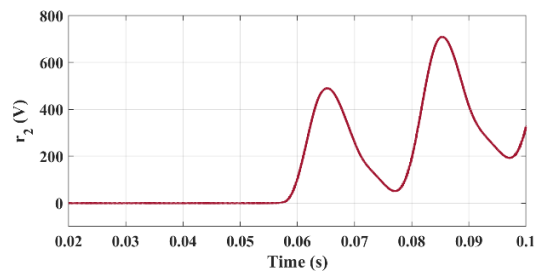


**Figure 17.** The residuals of the measured and estimated floating capacitor voltage of the faulty phase during the OCF.

The previous figures show the detection and identification of an OCF fault at the first cell by employing the load current and floating capacitor voltage. Figure 15 and Figure 17 depict the generation of the residuals of the measured and estimated signals; then, in Figure 18, we applied threshold values to the formed residuals to generate the detection signals.

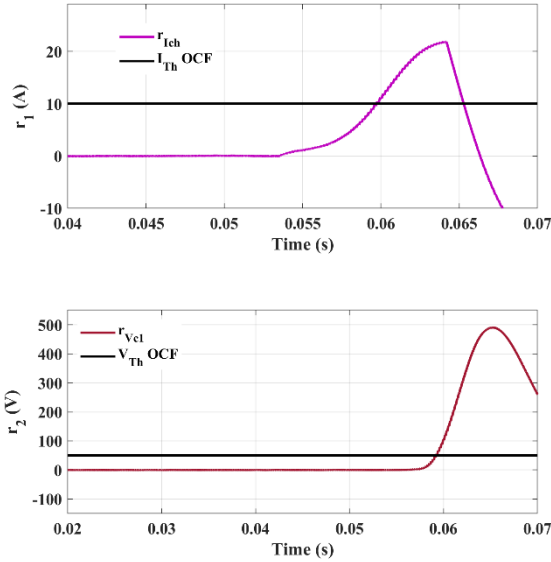


**Figure 18.** Residual and thresholds values for load current and floating capacitor voltage during OCF.

The results clearly illustrate the usefulness of the proposed observer in detecting and identifying switching faults during an OCF fault.

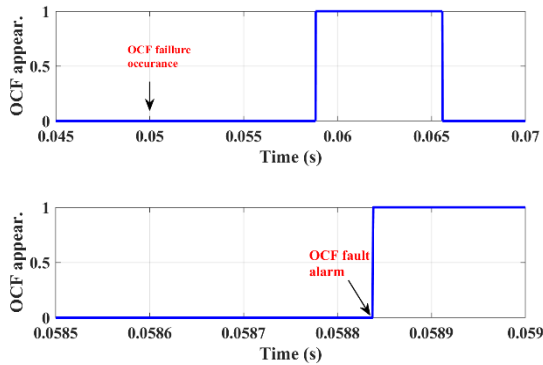


**Figure 19.** OCF fault detection time.

In Figure 19, OCF failure occurrence is defined as the moment when the open circuit fault occurs, at  $t=0.05$  (s). The OCF fault alarm is triggered when the residual first crosses the threshold, at  $t_{\text{alarm}} \approx 0.058$  (s). Therefore, the OCF detection time is  $t_{\text{det}} \approx 0.008$  (s).

Given the importance and critical nature of SCF faults in this type of inverter, it is essential to ensure the

reliability of the SCF fault detection approach. The following figures illustrate the results of SCF fault detection

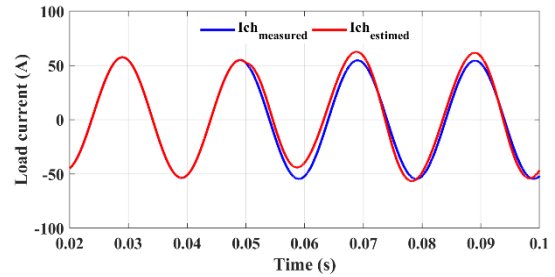


**Figure 20.** the measured and estimated load current of the faulty phase during SCF.

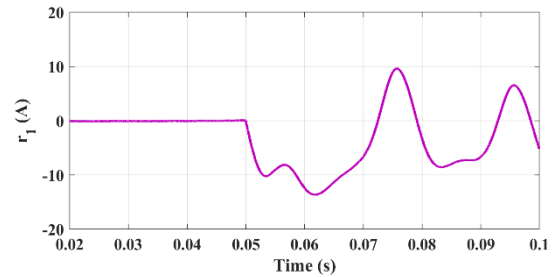


**Figure 21.** The residuals of the measured and estimated load current of the faulty phase during the OCF.

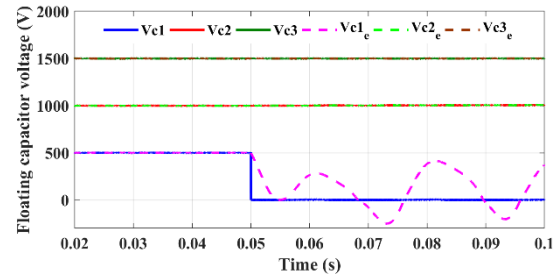


**Figure 22.** The measured and estimated voltages of the floating capacitors of the faulty phase during SCF.

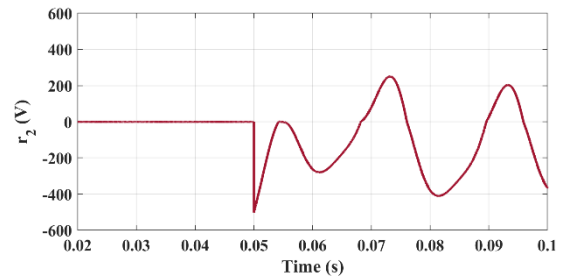


**Figure 23.** The residuals of the measured and estimated floating capacitor voltage of the faulty phase during the SCF.

In the scenario of an SCF fault occurring at time  $T_1$  in the IGBT corresponding to the first cell in phase (a) of the three-phase inverter, significant distortions in the output's voltages and currents, as depicted in Figure 13, Figure 20,

and Figure 22, indicate a degraded regime. The previous figures illustrate the measured and estimated signals of the load current and the voltage of the floating capacitors of the faulty phase of the three-phase inverter, Figure 21 and Figure 23 illustrate the generation of the residual signal. In Figure 24, we applied threshold values to the formed residuals to generate the detection signals.

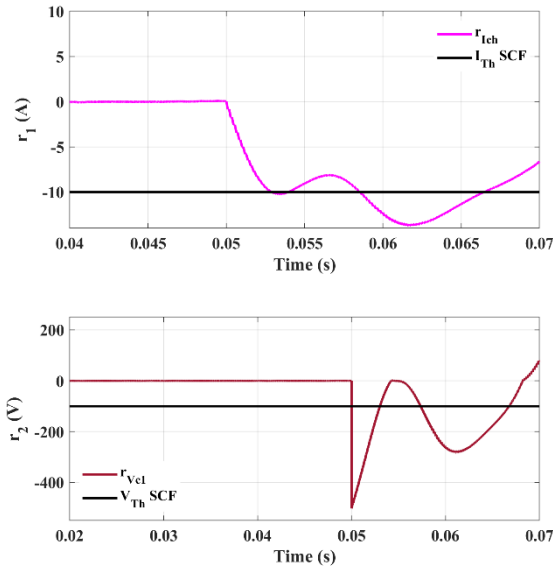


**Figure 24.** Residual and thresholds values for load current and floating capacitor voltage during SCF.

The detection signals are shown in the following Figure.

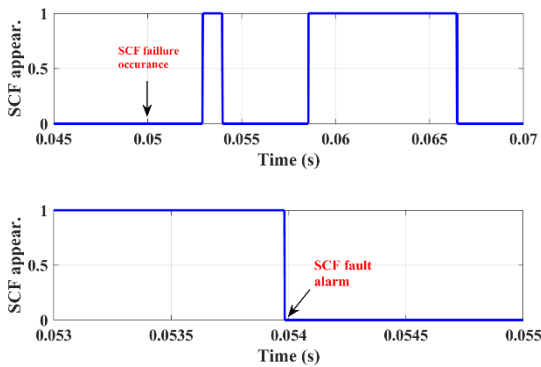


**Figure 25.** SCF fault detection time.

In Figure 25, SCF failure occurrence, at  $t=0.05$  (s). The OCF fault alarm is  $t_{alarm} \approx 0.054$  (s). Therefore, the SCF detection time is  $t_{det} \approx 0.004$  (s).

In the previously presented simulation analysis, the figures illustrate the characteristic signals for each type of failure and determine the fault diagnosis time for both OCF and SCF. As observed, the fault detection time for both types of faults is less than 10 (ms), indicating a fast

detection process. In [27], a comparison of fault diagnosis methods for three-phase inverters is presented and summarized. The fault diagnosis time based on signal processing exceeds 20 (ms). In summary, the sliding mode observer-based diagnosis method proposed in this paper enhances fault detection and localization speed by up to 50% through residual performance.

During the fault detection phase, a fault alarm is triggered to indicate the presence of a fault in the phase without providing information about the specific component problem or fault mode. Thus, during the fault identification phase, the faulty cell and the type of fault that caused the alarm must be determined. This combined process of fault detection and identification is generally called "fault diagnosis," which aims to determine the nature, location, and type of fault. The next step is fault isolation, which may involve disabling or bypassing the faulty component while ensuring the rest of the system remains operational.

## 5. Conclusion

This paper presents a novel approach for diagnosing open-circuit faults (OCFs) and short-circuit faults (SCFs) in a three-phase multicell inverter. The primary objective of this study is to develop an effective fault diagnosis method for the analyzed converter. We have designed an innovative diagnostic approach using a sliding mode observer. By comparing the residuals generated by the observer against a predefined threshold, we achieved precise detection and localization of both open- and short-circuit switch faults. Furthermore, this method identifies the nature of the fault and the exact faulty switch, ensuring a robust and efficient fault diagnosis. The fault diagnosis method based on the sliding mode observer provided a key advantage: it significantly reduced the false alarm rate by enhancing the system's resilience to fluctuations in the IGBT power supply. This robustness ensured reliable fault detection, minimizing erroneous alerts and improving system performance. The obtained results demonstrated the effectiveness of the proposed technique in accurately detecting and identifying both open-circuit and short-circuit faults within the converter. The results validated the proposed approach's reliability as a robust fault diagnosis solution. The sliding mode observer method demonstrated remarkable speed and efficiency in fault diagnosis while minimizing its impact on the overall



system operation, ensuring rapid detection and seamless performance.

Furthermore, the implementation of sliding mode control proved highly effective, highlighting its advantages in optimizing the inverter's performance by enhancing stability, increasing reliability, and ensuring robust operation under various conditions. The controller demonstrated stable and robust performance, significantly reducing static error and enhancing response time. These improvements make it an effective control strategy for boosting inverters' overall performance and reliability.

After a successful fault diagnosis, selecting an adequate fault-tolerant control method became paramount. Fault-tolerant control is crucial for maintaining the reliability and robustness of power systems that incorporate multilevel-multicell converters, ensuring continued performance even in the presence of faults. The task involved formulating control strategies that could swiftly identify and address faults within the power converter, enabling the system to remain operational and execute appropriate measures to mitigate the effects of the fault, ensuring minimal disruption to performance. We can recommend several fault-tolerant control strategies to ensure system functionality even in the presence of faults. One approach is redundancy-based control, where redundant power switches or control modules are added to provide backup functionality in case of failure. Another effective strategy is reconfiguration, which involves dynamically updating control parameters and altering the control structure in real time to adapt to fault conditions, thereby maintaining optimal system performance and reliability. Our future research will concentrate on the experimental evaluation and validation of the proposed fault diagnosis technique alongside developing and testing fault-tolerant control strategies. This strategy will ensure these methods' practical applicability and effectiveness in real time.

### Competing Interest Statement

The authors declare that they have no known competing financial interests or personal relationships that could have appeared to influence the work reported in this paper.

### Data Availability Statement

All data generated or analyzed during this study are included in this article.

### Author Contribution Roles

Research concept and design, F.K, A.A, S.F; Collection and/or assembly of data, A.A, F.K; Data analysis and interpretation, F.K, A.A, H.A; Writing the article, F.K, A.A, M.Z.D; Critical revision of the article, F.K, A.A, M.Z.D; Final approval of the article, A.A, S.F, H.A.

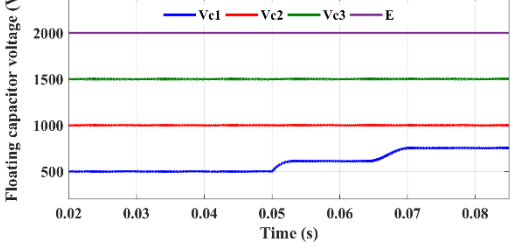
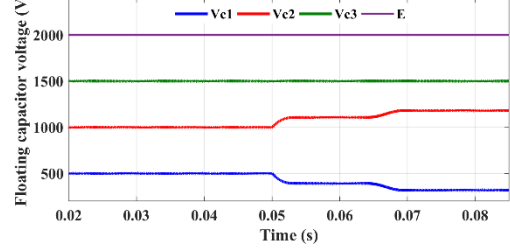
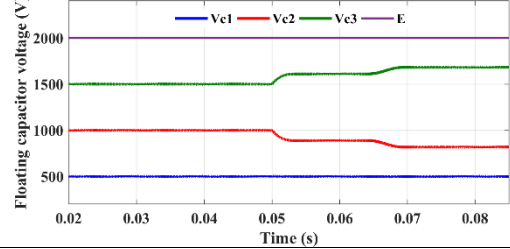
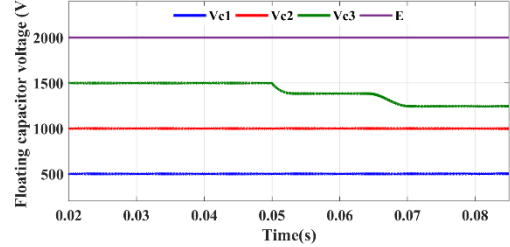
### References

- [1] K. Benmansour, A. Benalia, M. Djemai, J. de Leon, "Hybrid control of a multicellular converter," *Nonlinear Analysis: Hybrid Systems*, vol. 1, pp. 16-29, 2007, <http://doi:10.1016/j.nahs.2006.06.001>.
- [2] T.A. Meynard, H. Foch, "Multi-Level Choppers for High Voltage," *EPE Journal*, vol. 2, no. 1, pp. 45-50, March 1992, <http://doi:10.1080/09398368.1992.11463285>.
- [3] H. Toubakh, M. Sayed-Mouchaweh, M. Benmiloud, "Self-adaptive learning scheme for early diagnosis of simple and multiple switch faults in multicellular power converters," *ISA Transactions*, vol. 113, pp. 222-231, 2021, <http://doi:10.1016/j.nahs.2006.06.001>.
- [4] P. Djondiné, "Overview of control techniques for multicellular converter," *Journal of Engineering Sciences*, vol. 1, pp. E10-E14, 2018, [http://doi:10.21272/jes.2018.5\(1\).e3](http://doi:10.21272/jes.2018.5(1).e3).
- [5] O. Benzineb, F.Taibi, T.M. Laleg-Kirati, M.S. Boucherit, M.Tadjine, "Control and faults diagnosis based sliding mode observer of a multicellular converter: Hybrid Approach," *Journal of Electrical Engineering*, vol. 64, no. 1, pp. 20-30, 2013, <http://doi:10.2478/jee-2013-0003>.
- [6] G. Gateau, M. Fadel, P. Maussion, R. Bensaid, T.A. Meynard, "Multicell Converters: Active Control and Observation of Flying-Capacitor Voltages," *IEEE Transactions on Industrial Electronics*, vol. 49, no. 5, pp. 998-1008, 2002, <http://doi:10.1109/TIE.2002.803200>.
- [7] O. Tachon, M.Fadel, T.Meynard, "Control of series multicell converter by linear state feedback decoupling," *7th European Conference on Power Electronics and Applications EPE*, Trondheim, Norway, September 1997.
- [8] W. Perruquetti, J.P. Barbot, "Sliding mode control in engineering," *Marcel Dekker, Inc*, 2002.
- [9] F. W. Fuchs, "Some diagnosis methods for voltage source inverters in variable speed drives with induction machines

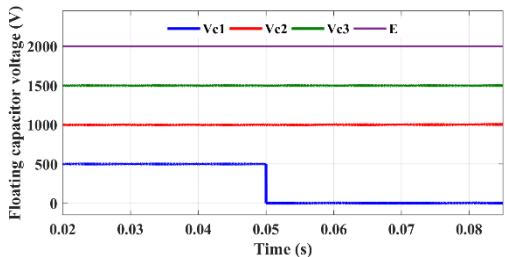
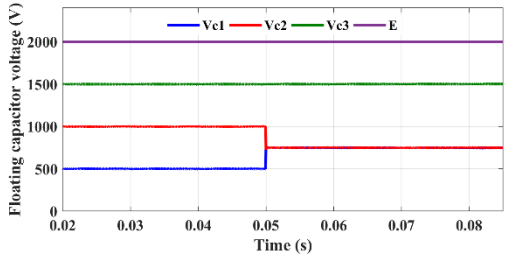
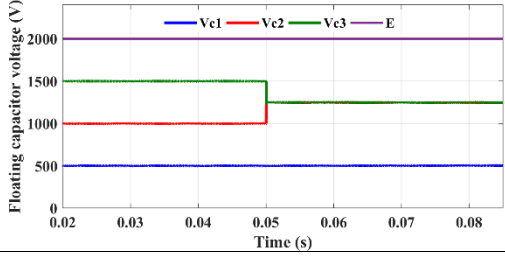
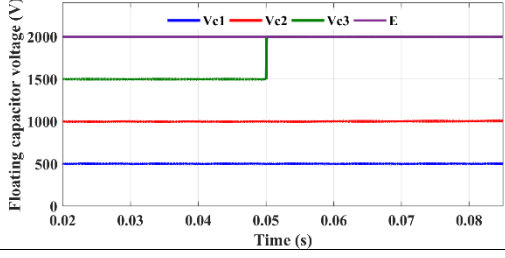
- a survey," *IECON'03, Roanoke, VA, USA*, pp. 1378-1385, 2003, <http://doi.org/10.1109/IECON.2003.1280259>.
- [10] A. Aibeche, M. Kidouche, "Sensor fault detection, localization, and system reconfiguration with a sliding mode observer and adaptive threshold of PMSM," *J. Power. Electron*, Vol. 16, no. 3, pp. 1012–1024, 2016, <http://dx.doi.org/10.6113/JPE.2016.16.3.1012>.
- [11] G. K. Kumar, D. Elangovan, "Review on fault-diagnosis and fault-tolerance for DC–DC converters." *IET Power Electronics*, vol. 13, pp. 1-13, 2019, <http://doi.org/10.1049/iet-pel.2019.0672>.
- [12] F. Khater, A. Aibeche, S.A. Fellag, M.Z. Doghmane, H. Akroum, "Failure identification and isolation of DC-DC boost converter using a sliding mode controller and adaptive threshold," *Diagnostyka*, vol. 25, no 03, pp. 1-15, 2024, <http://doi.org/10.29354/diag/190318>.
- [13] C. Chen, Y. Yang, B. Zhang, S. Gao, "The Diagnostic Method for Open-Circuit Faults in Inverters Based on Extended State Observer," *Mathematical Problems in Engineering*, 2021, <https://doi.org/10.1155/2021/5526173>.
- [14] C. Drif, A. Soualhi, H. Nouri, "A technique for diagnosing short-circuit and open-circuit faults of the three-phase inverter," *19th International Multi-Conference on Systems, Signals & Devices*, Sétif, Algeria, 2022, <http://doi.org/10.1109/SSD54932.2022.9955675>.
- [15] S. Meradi, K. Benmansour, K. Herizi, M. Tadjine, M.S. Boucherit, "Sliding mode and faults tolerant control for multicell converter four quadrants," *Electric Power Systems Research*, vol. 95, pp. 128-139, 2013, <https://doi.org/10.1016/j.epsr.2012.08.014>.
- [16] S. Shao, P.W. Wheeler, Clare JC, A.J. "Watson, Open-circuit fault detection and isolation for modular multilevel converter based on sliding mode observer," *15th European Conference on Power Electronics and Applications EPE*, 2013, <https://doi.org/10.1109/EPE.2013.6634401>.
- [17] A. El Mekki, K. Ben Saad, "Fault diagnosis of open and short-circuit faults in a parallel multi-cell converter based on sliding mode observer," *SN Appl. Sci.*, vol. 2, no. 179, 2020, <https://doi.org/10.1007/s42452-020-1954-6>.
- [18] F. Khater, A. Aibeche, S. A. Fellag, "Faults diagnosis for multilevel-multicell Converters using sliding mode controller and adaptive threshold," *ICAECOT*, Setif, Algeria, 2024, <http://doi.org/10.1109/ICAECOT62402.2024.10829285>.
- [19] B.J. Hyon, D.Y. Hwang, P. Jang, Y.-S. Noh, J.-H. Kim, "Offline Fault Diagnosis for 2-Level Inverter: Short-Circuit and Open-Circuit Detection," *Electronics*, vol. 13, no. 9, <https://doi.org/10.3390/electronics13091672>.
- [20] T. A. Meynard, M. Fadel, N. Aouda, "Modeling of Multilevel Converters," *IEEE Transactions on Industrial Electronics*, vol. 44, no. 3, JUNE 1997, <http://doi.org/10.1109/41.585833>.
- [21] K. Taniguchi, Y. Ogino, H. Irie, "PWM technique for power MOSFET inverter," in *IEEE Transactions on Power Electronics*, vol. 3, no. 3, pp. 328-334, July 1988, <https://doi.org/10.1109/63.17951>.
- [22] S. Ben Said, K. Ben Saad, M. Benrejeb, "On two control strategies for multicellular converters," *International Journal of Control, Energy and Electrical Engineering (CEEE)*, vol. 1, pp. 37-42, 2014.
- [23] H. Komurcugil, S. Biricik, S. Bayhan and Z. Zhang, "Sliding Mode Control: Overview of Its Applications in Power Converters," in *IEEE Industrial Electronics Magazine*, vol. 15, no. 1, pp. 40-49, March 2021, <https://doi.org/10.1109/MIE.2020.2986165>.
- [24] L. Wu, J. Liu, S. Vazquez and S. K. Mazumder, "Sliding Mode Control in Power Converters and Drives: A Review," in *IEEE/CAA Journal of Automatica Sinica*, vol. 9, no. 3, pp. 392-406, March 2022, <https://doi.org/10.1109/JAS.2021.1004380>.
- [25] C. Edwards, S. K. Spurgeon, R. J. Patton, "Sliding mode observers for fault detection and isolation," *Automatica*, Vol. 36, no. 4, 2000, [https://doi.org/10.1016/S0005-1098\(99\)001776](https://doi.org/10.1016/S0005-1098(99)001776).
- [26] R. Bensaid, M. Fadel "Sliding mode observer for multicell converters," *5<sup>th</sup> IFAC Symposium on Nonlinear Control Systems*, SI. Petersburg, Russia, 2001.
- [27] B. Lu, S. K. Sharma, "A Literature Review of IGBT Fault Diagnostic and Protection Methods for Power Inverters," in *IEEE Transactions on Industry Applications*, vol. 45, no. 5, pp. 1770-1777, 2009, <https://doi.org/10.1109/TIA.2009.2027535>.

## 6. Appendix

**Table 2.** Floating capacitor voltages for various Cases of OCF.

Fault description	The voltage of the floating capacitors	Notes
The OCF fault has occurred on the IGBT corresponding to the 1st cell.		The voltage across the first floating capacitor ( $V_{c1}$ ) undergoes an increase at the time of the fault. These increments initiate at 20% and can reach up to 60% of their value throughout the simulation period.
The OCF fault has occurred on the IGBT corresponding to the 2nd cell.		The voltage across the second floating capacitor ( $V_{c2}$ ) experiences increments reaching 20% (+200 V) of its value. Conversely, the voltage across the adjacent capacitor ( $V_{c1}$ ) undergoes a decline of 40% (-200 V) of its value from the moment of the fault and throughout the simulation period.
The OCF fault has occurred on the IGBT corresponding to the 3rd cell.		The voltage across the third floating capacitor ( $V_{c3}$ ) rises by up to 13.4% (+200 V) of its value. In contrast, the voltage across the adjacent capacitor ( $V_{c2}$ ) experiences a decrease of 20% (-200 V) Throughout the duration from the moment the fault occurs until the end of the simulation period.
The OCF fault has occurred on the IGBT corresponding to the 4th cell.		The voltage across the capacitor ( $V_{c3}$ ) decreases by 20% from the moment of the fault and throughout the simulation period.

**Table A2.** Floating capacitor voltages for various Cases of SCF.

Fault description	The voltage of the floating capacitors	Notes
The SCF fault has occurred on the IGBT corresponding to the 1st cell.		The voltage across the first floating capacitor ( $V_{c1}$ ) undergoes an abrupt drop to zero (-500V). Other voltages are not affected by any changes.
The SCF fault has occurred on the IGBT corresponding to the 2nd cell.		The voltage across the second floating capacitor ( $V_{c2}$ ) experiences a sharp drop of up to 25% (-250 V) of its value. In contrast, the voltage across the adjacent capacitor ( $V_{c1}$ ) undergoes a sudden increase in its value of 50% (+250 V).
The SCF fault has occurred on the IGBT corresponding to the 3rd cell.		The voltage across the floating capacitor ( $V_{c3}$ ) undergoes an abrupt decrease of 16.7% (-250 V). Conversely, the voltage across the adjacent floating capacitor ( $V_{c2}$ ) increases by up to 25% (+250 V) of its value.
The SCF fault has occurred on the IGBT corresponding to the 4th cell.		The voltage across the floating capacitor $V_{c3}$ undergoes an abrupt increase of 33.4% (+500 V).